



HAL
open science

An estimation of the electrical characteristics of planetary shallow subsurfaces with TAPIR antennas

Alice Le Gall, Alain Reineix, Valérie Ciarletti, Jean-Jacques Berthelier, R. Ney, F. Dolon, Charlotte Corbel

► **To cite this version:**

Alice Le Gall, Alain Reineix, Valérie Ciarletti, Jean-Jacques Berthelier, R. Ney, et al.. An estimation of the electrical characteristics of planetary shallow subsurfaces with TAPIR antennas. *Journal of Geophysical Research. Planets*, 2006, 111 (E6), pp.E06S06. 10.1029/2005JE002595 . hal-00155628

HAL Id: hal-00155628

<https://hal.science/hal-00155628>

Submitted on 8 Jan 2018

HAL is a multi-disciplinary open access archive for the deposit and dissemination of scientific research documents, whether they are published or not. The documents may come from teaching and research institutions in France or abroad, or from public or private research centers.

L'archive ouverte pluridisciplinaire **HAL**, est destinée au dépôt et à la diffusion de documents scientifiques de niveau recherche, publiés ou non, émanant des établissements d'enseignement et de recherche français ou étrangers, des laboratoires publics ou privés.

An estimation of the electrical characteristics of planetary shallow subsurfaces with TAPIR antennas

A. Le Gall,¹ A. Reineix,² V. Ciarletti,¹ J. J. Berthelier,¹ R. Ney,¹ F. Dolon,¹ and C. Corbel¹

Received 9 September 2005; revised 21 February 2006; accepted 27 February 2006; published 30 June 2006.

[1] In the frame of the NETLANDER program, we have developed the Terrestrial And Planetary Investigation by Radar (TAPIR) imaging ground-penetrating radar to explore the Martian subsurface at kilometric depths and search for potential water reservoirs. This instrument which is to operate from a fixed lander is based on a new concept which allows one to image the various underground reflectors by determining the direction of propagation of the reflected waves. The electrical parameters of the shallow subsurface (permittivity and conductivity) need to be known to correctly determine the propagation vector. In addition, these electrical parameters can bring valuable information on the nature of the materials close to the surface. The electric antennas of the radar are 35 m long resistively loaded monopoles that are laid on the ground. Their impedance, measured during a dedicated mode of operation of the radar, depends on the electrical parameters of soil and is used to infer the permittivity and conductivity of the upper layer of the subsurface. This paper presents an experimental and theoretical study of the antenna impedance and shows that the frequency profile of the antenna complex impedance can be used to retrieve the geoelectrical characteristics of the soil. Comparisons between a numerical modeling and in situ measurements have been successfully carried over various soils, showing a very good agreement.

Citation: Le Gall, A., A. Reineix, V. Ciarletti, J. J. Berthelier, R. Ney, F. Dolon, and C. Corbel (2006), An estimation of the electrical characteristics of planetary shallow subsurfaces with TAPIR antennas, *J. Geophys. Res.*, *111*, E06S06, doi:10.1029/2005JE002595.

1. Introduction

[2] The extensive observations by the Viking spacecraft probes and more recently the high resolutions images from the Mars Global Surveyor camera [Malin and Edgett, 2000] have provided ample evidence of the former presence of liquid water on Mars. Indeed the valley networks bear striking analogies with valleys formed by runoff of surface water on Earth and gullies on crater walls or cliff sides appear similar to erosion features associated with water streams on terrestrial slopes [Baker, 2001]. These observations raise a number of fundamental questions on the geological and climatic history of Mars and the fate of the liquid surface water. If erosion of the atmosphere by interaction with the solar wind may account for the disappearance of a part of this water, it is thought that a significant amount of the former surface water may still be trapped in the subsurface under the form of ground ice or even liquid water at larger depths. Present models [Fanale et al., 1986; Squyres et al., 1992; Clifford, 1993] estimate that liquid water may exist at depths of ~ 1 to 3 km at the

equator and ~ 7 to 10 km in polar regions. Recent observations [Malin and Edgett, 2000] and models [Helbert and Benkoff, 2005] have raised the question of the existence of liquid water even much closer to the surface. Water on Mars is therefore one of the major questions that will be addressed by missions that will be flown to the planet in the future. Searching for water reservoirs was one of the objectives of the NETLANDER mission that was initiated in 1999 by CNES and unfortunately stopped in 2004. It foresaw the deployment of 4 small geophysical stations on the surface of the planet each including the TAPIR ground-penetrating radar which was proposed to explore the deep underground down to possibly 2 km. This instrument is based on a novel concept which allows one to get an image of the underground reflectors and is briefly described below.

[3] As shown by Ciarletti et al. [2003a], retrieving the propagation direction of the reflectors requires knowledge of the electrical characteristics of the subsurface which control the refraction of the electromagnetic waves exiting from the soil. Several methods have already been proposed in the field of electromagnetic investigation of subsurfaces to measure these parameters with particular emphasis on the measurement of the soil water content with a GPR [Van Overmeeren et al., 1997; Reppert et al., 2000; Huisman et al., 2003b; Lambot et al., 2004; Fratticcioli et al., 2004]. Huisman et al. [2003a] have given a general review of these works. The most commonly used methods are based on the Common MidPoint (CMP) or the Wide-angle Reflection and Refraction (WARR) techniques. The wave propagation

¹Centre d'Etudes des Environnements Terrestre et Planétaires (CETP/IPSL), Saint-Maur, France.

²XLIM/OSA/Projet CEM, Faculté des Sciences, Université de Limoges, Limoges, France.

velocity in the subsurface, hence the underground complex dielectric permittivity, can be extracted from multioffset GPR soundings (at a fixed central position for CMP, at a fixed transmitter position for WARR). Another widespread approach consists in determining the velocity of ground waves detected by GPR receivers. Electrical characteristics of the soil can also be deduced from the reflection coefficient of the air-soil interface although surface roughness may make this method quite inaccurate. None of these methods is appropriate to the case of a fixed radar, operating from the surface, in a monostatic mode. We have thus developed a new method which relies on the fact that the current distribution of an antenna laid on the ground, hence the antenna impedance, depends on the electromagnetic characteristics of the soil. Measuring the TAPIR antenna impedance thus give access to the electrical parameters of the underground.

[4] Following a brief description of the TAPIR instrument, we present an analytical and a numerical model of the antenna operation allowing the computation of the antenna impedance. Results of the detailed numerical simulations are compared to actual measurements made over sand, an arable soil and pure ice and used to derive the underground electric permittivity and conductivity. The inferred values are in good agreement with the direct laboratory measurements of permittivity and conductivity of soil samples or the well known properties of ice.

2. Description of TAPIR Ground-Penetrating Radar

[5] The radar and its operations have been described in detail in previous papers [Berthelier *et al.*, 2000, 2003; Ney *et al.*, 2003] and its principle and main characteristics will be briefly recalled here.

2.1. Instrument Concept

[6] TAPIR is a pulsed polarimetric ground-penetrating radar which operates at low frequencies, from 2 to ~6 MHz, in order to reach kilometric depths in the Martian subsurface. This range of frequencies offers a good compromise between the desired sounding range and a still realistic size of electrical antennas (35 meters). Ordinary ground-penetrating radars achieve a 3D imaging of the subsurface by performing measurements from a number of locations on the surface. Since TAPIR was to operate on a fixed lander and thus from a single location, a novel concept was proposed allowing determination of not only the distance but also the direction of the reflectors, thus providing a 3D imaging of the underground structures. The direction of the reflectors is deduced from the propagation vector of the reflected waves which can be retrieved from the analysis of 2 horizontal electric components and 3 magnetic components of the waves [Ciarletti *et al.*, 2003a]. Long range soundings require an extremely high sensitivity that can be achieved by a sophisticated onboard processing of the signal such as biphasing at transmission and coherent integrations at reception (up to 2^{31} in the present design). The radar also performs polarimetric observations that bring valuable information on the detailed characteristics of single reflectors such as boulders or on reflecting interfaces.

[7] Several modes of operation were anticipated on NET-LANDER. In addition to the nominal radar mode and the background mode to measure the HF radio electric ambient noise, the permittivity operating mode is devoted to the determination of the antenna impedance as a function of frequency by measuring the current and voltage at the base of the antenna during continuous ($\sim 10 \mu\text{s}$) transmission at several frequencies. In this paper, we will focus on this last mode.

2.2. Electrical Antennas

[8] Several types of antennas are used in GPR: resistively loaded dipole, bow-tie antenna, TEM horn, spiral antenna and impulse radiating antenna [Lighthart *et al.*, 2002]. As the antenna dimension is commensurate to the wavelength, only wire antennas were adequate for TAPIR.

[9] The instrument is equipped with two horizontal electric dipoles, orthogonal to each other that are used for both transmission and reception. As often used in high frequency impulse radars [Kanda, 1978], these antennas are broad band resistively damped half-wave dipoles. The broad band is required to transmit short pulses with minimum distortion and the resistive antenna profile damps out natural resonances, allowing us to maintain the radar blind zone to less than ~80 meters in our case. The loading profile adopted for TAPIR dipoles is derived from the work of Wu and King [1965] and Shen and King [1965] and expressed as

$$z_0(x) = \frac{\xi_0}{2\pi} \frac{\psi_0}{L-x} \quad (1)$$

z_0 is the theoretical impedance as a function of the position x along the antenna, L , the length of the antenna, $\xi_0 = \sqrt{\frac{\mu_0}{\epsilon_0}} = 120 \pi \Omega$, the free space impedance and ψ_0 , a complex constant depending on the antenna geometry (length L and radius a in the case of a wire antenna), the operating frequency and the free space wave number k_0 . Here, each monopole is 35 meters long (half wave dipoles at the frequency of 2 MHz for a relative permittivity of 4) and $\psi_0 = 17.63 - 2.43j$.

[10] This profile is optimized for free space and the traveling wave has an amplitude which decays linearly along the antenna. In theory, the current goes to zero at the ends of the antenna. At the expense of a nonnegligible loss in efficiency, the resulting 3 dB bandwidth extends from 100 kHz to 8 MHz.

3. Analytical Model of the Antenna Operation

[11] The antenna characteristics play a key role in the performances of ground-penetrating radars to detect buried objects or layers. GPR antennas are disposed close or directly on the surface and their characteristics vary with respect to ground electromagnetic nature. Although this coupling appears as a difficulty to ensure steady performances irrespective of experimental conditions, it may, on the other hand, be used to determine the electromagnetic properties of the soil.

[12] In this section, we will establish the analytical expression of the current distribution and of the antenna input impedance. We assume that dipoles are excited by

harmonic signals and that they lay on a semi-infinite homogeneous medium.

3.1. Constitutive Parameters of the Propagation Medium

[13] The interaction of harmonic electromagnetic waves with a linear isotropic homogeneous medium can be completely characterized if three scalar constitutive parameters of the medium are known [King and Smith, 1981]: the effective electric conductivity σ_e , the effective electric permittivity ϵ_e and the permeability μ . The electric permittivity (often referred to as the dielectric constant) is expressed as $\epsilon_e = \epsilon_r \epsilon_0$ where ϵ_r is the relative permittivity. The present study was conducted assuming that the underground magnetic permeability is equal to μ_0 since measurements were performed on nonmagnetic grounds. In the case of Mars, both Viking Landers and the Pathfinder Lander/Sojourner Rover brought evidence of the presence of magnetic minerals on the Martian surface [Hargraves et al., 1977], the red color of the planet also suggesting that it contains iron oxides (hematite, magnetite) [Heggy et al., 2001; Leuschen et al., 2003]. However, in absence of reliable information on the Martian subsurface permeability [Ori and Oglioni, 1996] we started by assuming nonmagnetic materials with: $\mu = \mu_0$. The influence of the magnetic properties of the soil on the antenna radiation and its impedance will be the subject of a future work.

[14] Thus, assuming a $e^{j\omega t}$ time dependence, any linear isotropic homogeneous medium m can be defined by a wave number: $k_m = \beta_m + j\alpha_m = \omega(\mu\epsilon_{em})^{1/2} (1 + jp_{em})^{1/2}$ where $p_{em} = \frac{\sigma_{em}}{\omega\epsilon_{em}}$ is the effective loss tangent.

[15] The complex permittivity is given by $\epsilon_C = \epsilon_0\epsilon_C = \epsilon_e - j\frac{\sigma_e}{\omega}$.

[16] Most of natural dry materials have very low conductivities (less than 10^{-4} S/m) and a relative dielectric constant lying in the range of 2 (sandstone. . .) to 10 (calcite, marble . . .). In contrast, liquid water displays very high values for both these parameters. Since we were interested in probing the Martian soil, our investigation, both theoretical and experimental, were limited to the case of low moisture with $\sigma_e < 10^{-3}$ S/m.

3.2. Coupling of TAPIR Antenna With the Subsurface

[17] As mentioned above, most of the work that have been undertaken on the coupling of antennas with the soil [King and Smith, 1981; Lestari et al., 2000; De Jongh et al., 1998] aimed at optimizing the antenna radiation pattern or finding solution to reduce this coupling and make easier the data interpretation. Besides, virtually no attention was paid to the case of loaded dipoles which have a specific behavior.

[18] We have first developed an analytical model of antenna operation which, in spite of its simplicity, provides a good insight on the physics of the coupling and especially on the role of the various parameters.

3.2.1. Wave Velocity Along the Antenna

[19] The harmonic wave propagation along a thin wire with $L \gg a$ lying on a plane interface between two nonmagnetic homogeneous media of wave numbers k_1 and k_2 has been studied by Wait [1972]. It is determined by the effective conductivity and permittivity that are equal

to the average values of these parameters in the upper and lower media:

$$k_{eq} = \left(\frac{k_1^2 + k_2^2}{2} \right)^{1/2} \quad (2)$$

Thus, at the interface between underground and air,

$$\epsilon_{req} = \frac{\epsilon_{r1} + \epsilon_{r2}}{2} = \frac{\epsilon_{rground} + 1}{2} \quad (3)$$

$$\sigma_{eq} = \frac{\sigma_1 + \sigma_2}{2} = \frac{\sigma_{ground}}{2} \quad (4)$$

In particular, the wave velocity in the antenna is given by the real part of the wave number:

$$v = \frac{k_0}{\beta_{eq}} \times c \quad \text{where} \quad \beta_{eq} = \text{Re}(k_{eq}) \quad (5)$$

A parametric study of v (as a function of $\epsilon_{rground}$ and σ_{ground}) and its comparison with measurement can thus be used to get insight into the electrical parameters of the subsurface materials.

3.2.2. Spatial Distribution of the Current

[20] The current amplitude behavior along the antenna is determined both by the surrounding medium properties and by the antenna resistive profile.

[21] As already mentioned, the resistive profile of the antenna $z_0(x)$ is optimized for free space. Thus the harmonic solution for the current along the dipole in free space must satisfy the differential equation (except at the driving point) [Wu and King, 1965]

$$\left(\frac{\partial^2}{\partial x^2} + k_0^2 - \frac{j2k_0}{L-x} \right) I(x) = 0 \quad (6)$$

Its solution is a wave of current traveling in the direction of increasing $|x|$ from the generator up to both ends; there is no reflected wave. The analytical expression of the current is

$$I_0(x) = -\frac{2\pi V_0^e}{\xi_0 \Psi_0 \left[1 - \frac{j}{k_0 L} \right]} \left(1 - \frac{|x|}{L} \right) e^{-jk_0|x|} \quad (7)$$

where V_0^e is the driving voltage.

[22] However, in our case, the antennas are laid on the ground and thus not in free space and the actual current profile differs from the simple linear solution of Wu and King. To establish an analytical expression of this current distribution, one must notice that the optimized distributed resistive loading for the real case should be:

$z_m(x) = \frac{\xi_m}{2\pi} \frac{\Psi_m}{L-x}$ where $\xi_m = \frac{\omega\mu_0}{k_m}$ and Ψ_m is computed for the medium wave number k_m . If TAPIR antennas had such a profile, equation (6), with k_m instead of k_0 , would be valid. But, as they have been optimized for free space, one must introduce a coefficient in this differential equation, the ratio

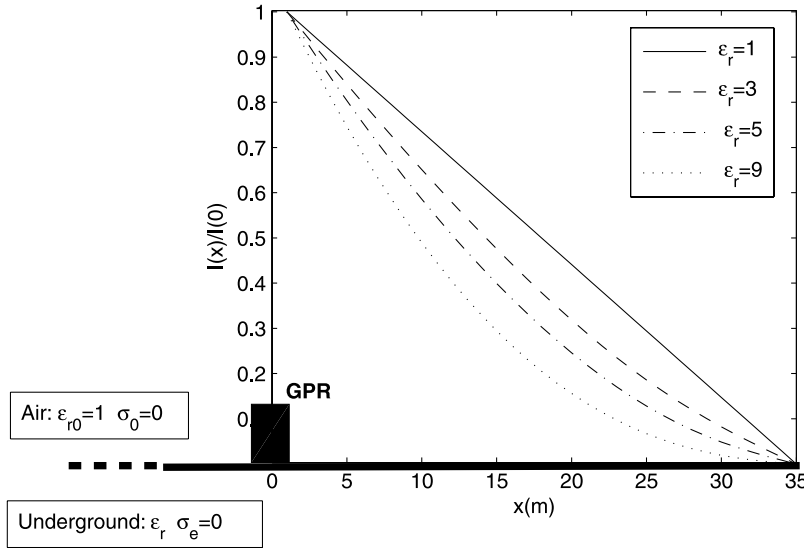


Figure 1. Current distribution along the antenna as a function of the relative permittivity of the subsurface ϵ_r . The conductivity of the subsurface, σ_e , is assumed to be zero.

(possibly complex) between the actual and the optimized profile [Wright and Prewitt, 1975]: $\delta_m = z_0(x)/z_m(x)$.

$$\delta_m = \delta_m(\omega) = \frac{\xi_0 \Psi_0}{\xi_m \Psi_m} \quad (8)$$

The wave equation (except at the driving point) becomes

$$\left(\frac{\partial^2}{\partial x^2} + k_m^2 - \frac{j2k_m \delta_m}{L-x} \right) I(x) = 0 \quad (9)$$

Wu and King solution (equation (7)) conforms to the case: $\delta_m = 1$.

[23] The cases where δ_m is lower than 1 and where δ_m is a positive integer have been treated by Wu and Shen [1967].

[24] The general case has been investigated, for a different purpose, by Wright and Prewitt [1975], who gave the following analytical solution:

$$I_m(x) = I_m(0) \left(1 - \frac{x}{L} \right) e^{-k_m x} \frac{M(1 - \delta_m, 2; -2jk_m(L-x))}{M(1 - \delta_m, 2; -2jk_m L)} \quad (10)$$

where M stands for the Kummer's functions.

At the driving point,

$$I_m(0) = \frac{2\pi}{\xi_m \Psi_m} \left(1 - \frac{j}{k_m L} - 2 \frac{M'(1 - \delta_m, 2; -2jk_m L)}{M(1 - \delta_m, 2; -2jk_m L)} \right)^{-1} \quad (11)$$

where

$$M'(c_1, c_2; z) \equiv \frac{\partial M(c_1, c_2; z)}{\partial z}.$$

[25] Expression (11) allows us to assess the influence of the electrical parameters of the antenna environment on the spatial current distribution. In our case, these parameters are obtained as averaged values of the air and in the soil.

[26] Figure 1 displays the decay of the current intensity along the antenna for a frequency of 4 MHz with the relative dielectric constant of the close subsurface ϵ_r as a parameter. The conductivity is assumed to be equal to zero. The nonlinearity of the current variation increases with the effective permittivity.

[27] Figure 2 displays the case of a conductivity of $2 \cdot 10^{-4}$ S/m. Curves in Figure 2 show that a higher conductivity increases the nonlinearity of the current profile along the antenna.

[28] Figures 1 and 2 thus provide evidence that the EM properties of the subsurface have a definite influence on the characteristics of the antenna. Thus measurements of the phase and amplitude of the current along the antenna can yield detailed information on the surrounding medium.

[29] While such measurements can be performed in terrestrial applications, it is obvious that they are out of scope for planetary missions. The determination of the antenna self impedance is far more practical since only two measurements (current and voltage) are needed. We have thus investigated the dependence of the antenna impedance on the underground geoelectrical parameters.

3.3. Influence of Subsurface Characteristics on Antenna Impedance

[30] The antenna impedance can be defined as the impedance at the driving point: $Z_a = Z_m(0) = \frac{V_0^e}{I_m(0)}$.

[31] Hence, for a medium m ,

$$Z_a = \frac{\xi_m \Psi_m}{2\pi} \left(1 - \frac{j}{k_m L} - 2 \frac{M'(1 - \delta_m, 2; -2jk_m L)}{M(1 - \delta_m, 2; -2jk_m L)} \right) \quad (12)$$

This expression is identical to that of Wu and King [1965] for $\delta_m = 1$.

[32] The frequency profile of the antenna impedance and its dependence on the permittivity ϵ_r of the underground is shown in Figure 3 for a conductivity equal to zero. The real

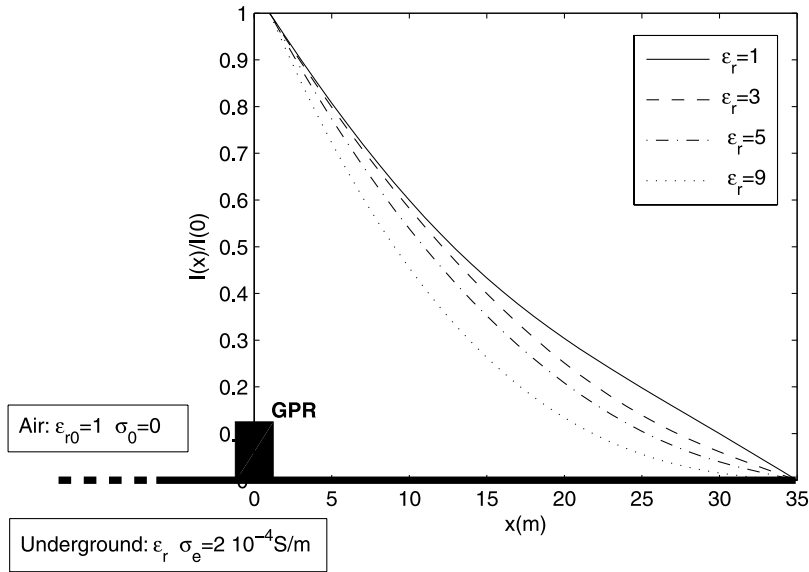


Figure 2. Current distribution along the antenna as a function of the relative permittivity of the shallow subsurface ϵ_r . The conductivity of the subsurface, σ_e , is assumed to be $2 \cdot 10^{-4}$ S/m.

part of the antenna impedance decreases with increasing permittivity whereas the imaginary one increases. Above 3 MHz, the impedance shows weak frequency variations and the antenna impedance is essentially determined by soil permittivity. The real part of the impedance is quite sensitive to this value while the imaginary part is less affected by permittivity variations. For ϵ_r from 1 to 9, the real part increases by nearly 350Ω while an increase of 200Ω is observed on the imaginary part.

[33] Figure 4 displays a similar diagram for several conductivities and a constant relative permittivity equal to 4. The sensitivity of the impedance with respect to the conductivity remains small except in the low frequency region, below 1 MHz.

[34] In conclusion, the analytical approach gives evidence of the influence of the electrical properties of the soil on the antenna behavior. The variations of the impedance measurements in response to changes in the permittivity and conductivity, in the lower frequency range, are large enough to allow retrieval of both parameters (with less accuracy from the conductivity) from a frequency profile of the antenna impedance. This motivated the development of a more realistic and accurate numerical model of the antenna operation.

4. Numerical Model of the Antenna Operation

[35] A numerical 3D FDTD code, TRIDIMO, has been developed by XLIM (formerly named IRCOM, Institut de Recherche en Communication Optique et Micro-Ondes) to simulate the operations of the GPR in an actual environment and, in particular, to determine the coupling between the antenna and the shallow subsurface with better accuracy than analytical models. This code has been described by Martinat [2001], Bauchet [2004], and Besse [2004] and will be the subject of a forthcoming paper (V. Ciarletti and A. Reineix, Ciarletti, V. and Reineix, A., Numerical simulation of a HF ground penetrating radar with the FDTD

method, manuscript in preparation, 2006). It takes into account the resistive profile of the antennas, the mutual cross coupling and the coupling with the lander structure. It also takes into account frequency dependence of the geoelectrical parameters.

4.1. FDTD Method

[36] The FDTD (Finite Difference Time Domain) method allows us to solve the set of Maxwell equations in a rigorous manner. The numerical algorithm is based on the well known Yee [1996] algorithm and relies on the discretization and resolution of Maxwell curl equations using a time stepping procedure [Martinat, 2001]. The advantages of this method lay in its relative simplicity of implementation, its accuracy and its versatility at the expense of a significant computation time. Stability conditions requires that the size of the discrete volume elements must be of the order of $\lambda/10$

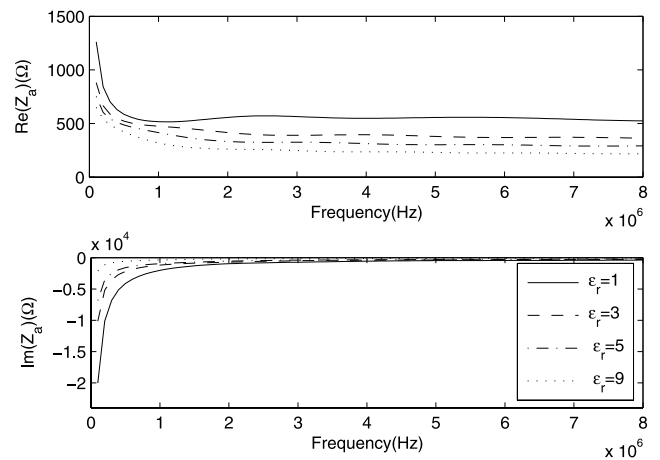


Figure 3. Frequency variations of the antenna impedance (computed with the analytical model) as a function of the relative permittivity of the shallow subsurface ϵ_r . The conductivity of the subsurface, σ_e , is assumed to be zero.

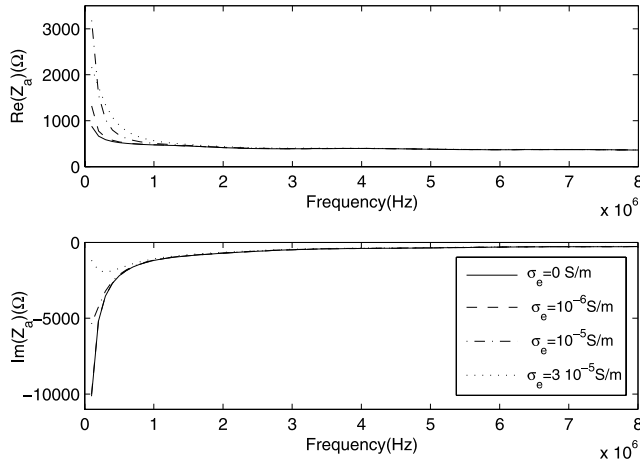


Figure 4. Frequency variations of the antenna impedance (computed by the analytical model) as a function of the conductivity of the shallow subsurface σ_e . The relative permittivity of the subsurface, ϵ_r , is assumed to be 4.

where λ is the wavelength in the medium corresponding to the highest frequency of operation (10 MHz). The chosen cell dimension is 1 meter in the three perpendicular directions which is small enough compared to the wavelength and prevents numerical dispersion. Besides, a relationship between the time and the spatial steps allows us to respect the CFL (Courant-Friedrichs-Levy) stability criterion. In addition, wave reflections on the walls of the computation box are suppressed by PML, “Perfectly Matched Layers” [Berenger, 1994; Berenger *et al.*, 2000] technique. An improved version of this method called CPML [Roden and Gedney, 1997] has been implemented to take into account more complex underground conditions such as lossy media.

4.2. Antenna Modeling

[37] Electrical antennas are thin metallic Mylar ribbons 35 meters long and 10 mm wide. To cope with computational cost issues, they have been modeled as thin cylindrical wires as proposed by Holland and Simpson [1981]. The corresponding algorithm relies on the following idea: since the radius of the antenna is negligible compared to the wavelength, electrostatic and magnetostatic laws are valid around the wire. Current and charge along the antenna can be derived and used as electrical sources in the Maxwell’s equations. As a consequence, no transverse discretization of the wire is required and the spatial increment remains appropriate to the volume size.

[38] The model allows us to insert local electrical elements (resistance, inductance, capacity. . .) on each segment of the antenna.

4.3. Soil Modeling

[39] The geoelectrical features of the soil are introduced in each cell of the 3D mesh representing the computation box through the desired values of the electric permittivity and conductivity. The code would also allow us to take into account the magnetic properties of the subsurface but, as

already indicated, we have, up to now, only considered the case of nonmagnetic materials.

[40] Due to the wide frequency bandwidth of the radar, the frequency variations of the electric parameters of the subsurface cannot be neglected. In the time domain, convolutions have to be performed asking for costly resources in memory and computational time. To cope with this issue, the permittivity frequency dependence is described by the classical Debye’s model [Luebbers *et al.*, 1990].

$$\epsilon_C(\omega) = \epsilon_\infty + \sum_{i=1}^N G_i \frac{(\epsilon_s - \epsilon_\infty)}{1 + j\omega\tau_i} \quad (13)$$

τ_i is the characteristic relaxation time of the dipole moment of the medium, ϵ_s is the static relative dielectric constant (maximum value) and ϵ_∞ a permittivity for an infinite frequency (minimum value). Permittivity is expressed as a sum of first order filters which lead to damping exponential terms in the time domain and thus to faster computation of the convolutions.

[41] As an example of the validity of the Debye model, we have performed laboratory measurements of the real and imaginary parts of the permittivity of a sample of sand from the Pyla Dune and fitted a Debye model with one pole for a conductive material. The corresponding expression is

$$\epsilon_C(\omega) = \epsilon_\infty + \frac{(\epsilon_s - \epsilon_\infty)}{1 + j\omega\tau_i} - j \frac{\sigma_s}{\omega\epsilon_0} \quad (14)$$

Values of $\epsilon_s = 5$ (DC or static permittivity), $\epsilon_\infty = 4$ (infinite frequency permittivity), $\tau_i = 0.8 \cdot 10^{-7}$ s (relaxation time) and $\sigma_s = 5 \cdot 10^{-5}$ S/m (DC or static conductivity) were found to give a very good agreement between measurements and model values, thus validating the Debye approximation.

4.4. Extent of the Soil Layer Controlling the Antenna Characteristics

[42] An important issue is to determine to which depth d_L the soil is electrically coupled to the antenna and affect its characteristics. One way to obtain this information is to analyze the variations of the antenna current as a function of the depth of the uniform soil beneath. This can be achieved by putting a perfectly reflecting plane at some depth in the computation box and computing the current flowing along the antenna. If the reflecting plane is very deep, the current due to the reflected electromagnetic field is negligible. When the distance from the plane to the surface is reduced, the current along the antenna is modified. d_L can be obtained as the depth of the reflecting plane where the change in the antenna current is negligible ($\sim 1\%$).

[43] The FDTD code was used to conduct this investigation in the case of an antenna laid on a dry sand ($\epsilon_r = 4$) and operating at the central frequency of 4 MHz. Numerical simulations made with a 5 cm spatial step revealed that for a depth of the reflector plane of ~ 1 m, the current is 20 dB below the transmitting current level. In near field domain, the transmitted waves are strongly attenuated in the vicinity of the dipole and the soil can be considered as electrically coupled to the antenna characteristics only down to a depth of ~ 1 m. A similar result was obtained over the whole range of frequencies of the radar.

[44] In conclusion the measurements of the antenna characteristics such as its impedance provide information on the EM properties of a thin layer of ~ 1 m beneath the surface.

5. Measurements and Comparison With Models: Determination of the Electrical Properties of the Shallow Subsurface

[45] In this section, we compare model simulations and measurements of the antenna characteristics performed during several field tests.

5.1. Soil Characteristics

[46] The antenna operation can be studied by measuring various parameters: the wave propagation velocity and the current profile along the antenna or, more simply, the antenna impedance.

[47] Wave propagation and current profile were measured over a rather dry arable soil, in the park of Saint-Maur Observatory, and over the Pyla sand dune, in the South of France. Antenna impedance measurements were performed on the Pyla dune and on the Antarctic ice shelf during the RANETA (RADar of NETlander in Terre Adélie) campaign [Bertheliet *et al.*, 2005].

5.1.1. Saint-Maur Observatory

[48] The Saint-Maur Observatory garden can be considered as an arable soil containing organic materials. Measurements on this site were performed in spring, in a rather dry period with no rain during the preceding week. The soil can thus be considered as rather dry.

[49] A sample was collected a few months later, in meteorological conditions similar to those encountered during the antenna tests. Measurements of the electromagnetic properties of the sample were performed with the impedance analyzer HP4192A in the PIOM laboratory (Laboratoire de Physique des Interactions Ondes-Matière). The analyzer instrument operates in the frequency range from 5 Hz to 13 MHz and provides the real and imaginary parts of the permittivity as a function of frequency. At the operating frequency of 4 MHz, the derived relative dielectric constant is ~ 5 and the effective conductivity is $\sim 10^{-3}$ S/m. Yet, one must keep in mind that these values can vary locally due to the natural inhomogeneity in the moisture and organic material contents. However, the measurements can be thought as representative of the average values of ϵ_r and σ_e with possible random deviations of 30%.

5.1.2. Pyla Dune

[50] With a height of 100 m, the Pyla Dune is the highest dune of Europe. It constitutes a suitable ground to test ground-penetrating radars since it is a quite homogenous and moderately lossy medium.

[51] Measurements of the electromagnetic properties of the sand of the Pyla Dune have been performed in the PIOM laboratory for a number of samples collected at various times, locations on the dune and depths below the surface. The relative permittivities of these samples range from 2.9 to 4.4 and the effective conductivity from 10^{-5} to 10^{-4} S/m [Ciarletti *et al.*, 2003b] at TAPIR operating frequencies (from 1 to 4 MHz).

5.1.3. Antarctic Ice Shelf

[52] The RANETA campaign took place in January/February 2004, over the Antarctic ice shelf, in Terre Adélie. The

electromagnetic properties of ice as a function of temperature and frequency are well known. They have been recently reviewed by Fujita *et al.* [2000]. Up to 600 MHz, the electromagnetic parameters are practically independent of frequency. The average temperature of the ice between the surface and the bedrock at the location of the measurements is estimated to $\sim -20^\circ\text{C}$. Typical values of the electric conductivity and of the relative dielectric constant are respectively $5 \cdot 10^{-5}$ S/m and 3.2 at this temperature. Besides, between $\sim -10^\circ\text{C}$ and $\sim -30^\circ\text{C}$, the relative permittivity is virtually unchanged and the conductivity remains low, between 10^{-6} and $3 \cdot 10^{-5}$ S/m.

5.2. Signal Propagation Along the Antenna

[53] The measurements were performed with a current transformer (Bergoz CT-C1.0) on 35 meters resistively loaded dipoles for long pulses ($>4 \mu\text{s}$, in order to install the required stationary mode) and at a central frequency of 4 MHz.

[54] The nominal accuracy of the CT is 0.5% in the wide bandwidth [200 Hz, 500 MHz], uncertainties on current measurement are thus very low.

5.2.1. Wave Propagation Velocity Along the Antenna

[55] During field tests at Saint-Maur Observatory, two independent data sets were acquired, one with the antennas lying on the surface, the second one with the antenna 1 meter above the surface. Measurements on the Pyla dune were only performed with the antenna directly laid on the surface.

[56] In the first case, with the antenna laid on the surface, the measured wave velocity is $\sim 1.78 \cdot 10^8$ m s $^{-1}$, whereas, one meter above the surface, the wave velocity is $\sim 2.56 \cdot 10^8$ m s $^{-1}$. This result is in good agreement with theory (see section 3.2.1); it shows that even 1 m above the surface, the soil has still a measurable influence on the antenna since the measured velocity is well below its value of $3 \cdot 10^8$ m s $^{-1}$ in free space. In Figure 5 we have plotted the computed ratio between the propagation constant in the antenna β_{eq} and the propagation constant in the air β_0 as a function of the electromagnetic properties of the near by soil (ϵ_r, σ_e) (see section 3.2.1). The thick line is the measured ratio: $\frac{\beta_{eq}}{\beta_0} = \frac{c}{v} \approx 1.68$.

[57] When the electric conductivity is less than $\sim 3 \cdot 10^{-4}$ S/m, it has practically no influence on the wave velocity which is uniquely determined by the relative dielectric constant ϵ_r . On the contrary, larger values of σ_e have a significant effect on the wave velocity. As can be seen on the curves in Figure 5, the pair (ϵ_r, σ_e) obtained on our sole sample can be matched with different solutions. Depending on which measurement, ϵ_r or σ_e , is supposed to be more accurate, one can obtain 2 extreme solutions: $\epsilon_r = 4.7 \pm 0.2$, $\sigma_e = 10^{-5}$ S/m or $\epsilon_r = 3.8 \pm 0.15$, $\sigma_e \sim 10^{-3}$ S/m. According to King and Smith [1981] the dielectric and conducting properties of a soil greatly depend on the moisture content. Typically, when dry, a soil may have relative permittivity ranging from 2 to 6 and conductivity between 10^{-5} and 10^{-4} S/m. Thus, since the soil is certainly rather dry, we can reduce the possible solutions for σ_e to: $10^{-4} \text{ Sm}^{-1} \leq \sigma_e \leq 10^{-5} \text{ Sm}^{-1}$.

[58] It must be also emphasized that, in garden environments such as in the park of Saint-Maur Observatory, the characteristics of the soil, moisture and organic contents,

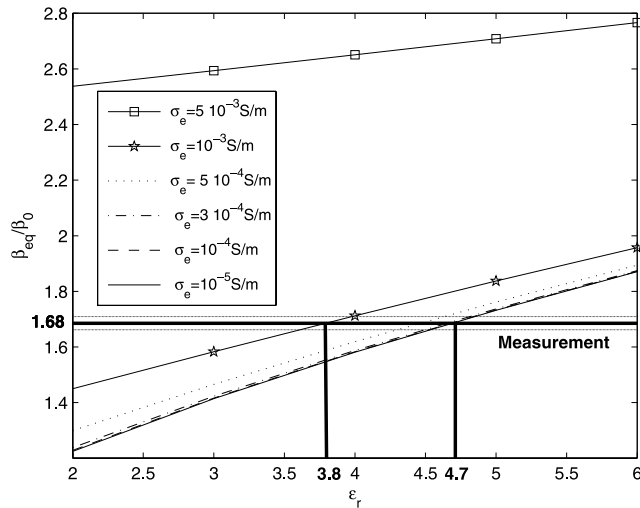


Figure 5. Wave propagation velocity along the antenna as a function of the relative permittivity ϵ_r and of the conductivity σ_e of the shallow subsurface. Comparison between analytical simulations and measurements performed at Saint-Maur Observatory (thick line).

may display large variations over distances of a few meters and depths of a few tens of centimeters. Very clearly, the 35 m length of the antenna and the ~ 1 m extent in depth of the soil layer coupled with the antenna would have required some ~ 10 samples to be taken in order to get representative average values of the electrical properties.

[59] To conclude, the analytical approach combined with measurements of the wave propagation speed acquisition brings a range of possible values for ϵ_r and σ_e . In our case, the best fit solution is: $\epsilon_r \sim 4.7 \pm 0.2$ and $\sigma_e \sim 10^{-4}$ S/m.

5.2.2. Current Profile

[60] Figure 6 displays the normalized amplitude decay of the measured current for three different cases, on the sand dune, on the garden soil and 1 meter above and theoretical curves from the analytical model are shown in thick lines.

[61] For the dry soil cases, a technical error in the measurements procedure makes the current measurements beyond 25 m inaccurate and thus they must be discarded. The curves are consistent with the analytical results that predict that an increase of the effective permittivity entails a more nonlinear variation of the current intensity along the antenna. For an antenna 1 meter above the soil, the current profile is quasi-linear, as expected since the conditions are closer to those in free space. By adjusting the parameters (ϵ_r , σ_e) in the analytical model, we have determined best fit values:

[62] 1. For the Pyla Dune: $\epsilon_r = 4.2$ and $\sigma_e = 3 \cdot 10^{-5}$ S/m.

[63] 2. For the air: $\epsilon_r = 1$ and $\sigma_e = 2 \cdot 10^{-5}$ S/m.

[64] 3. For the quite dry earth: $\epsilon_r = 4.8$ and $\sigma_e = 10^{-4}$ S/m.

[65] For the garden soil, there is a good agreement with the values of relative permittivity and conductivity deduced from the wave velocity and laboratory measurements. For the sand of the Pyla dune, these values are also consistent with those given by [Barbin, 1996; Bauchet, 2004] and with extracted values from the literature in the case of dry sand. They also provide satisfying fits when used in numerical model.

5.3. Antenna Impedance

[66] As stated above, impedance measurement are in practice the only way to determine the relative permittivity and conductivity of the upper layer of planetary soil. The impedance frequency profile also provides insight in the frequency dependence of the complex permittivity. Results shown just above have proved the ability of the analytical model to describe antenna characteristics at a single frequency but, in the case of a range of frequencies, the numerical model is far more suitable to data interpretation.

[67] Figure 7 shows the antenna impedance measured on the Pyla Dune in the frequency range 0.3 to 6 MHz and the corresponding analytical and numerical simulations obtained with a single pole Debye model of a conductive sand as indicated in section 4:

$$\epsilon_C(\omega) = 4 + \frac{(5-4)}{1 + 8 \times 10^{-8} \times j\omega} - j \frac{5 \times 10^{-5}}{\omega \epsilon_0}$$

[68] The localized increase of the impedance near 4 MHz is due to the presence of a parasitic broadcast transmitter. The analytical model relies on a simplified approach considering an isolated antenna with a continuously varying resistive profile. The FDTD code takes into account the actual antenna with discrete resistances between conductive segments and more importantly its coupling with the lander structure, the other antennas and the electronics. The resulting fit is very satisfying and provides evidence of the validity and accuracy of the numerical model.

[69] Similar numerical simulations have been achieved with a set of different values of the geoelectrical parameters. Figure 8 shows for example a 2D color diagram of the numerically computed real and imaginary parts of the antenna impedance at 1 MHz as functions of the relative permittivity and the conductivity of the subsurface. Com-

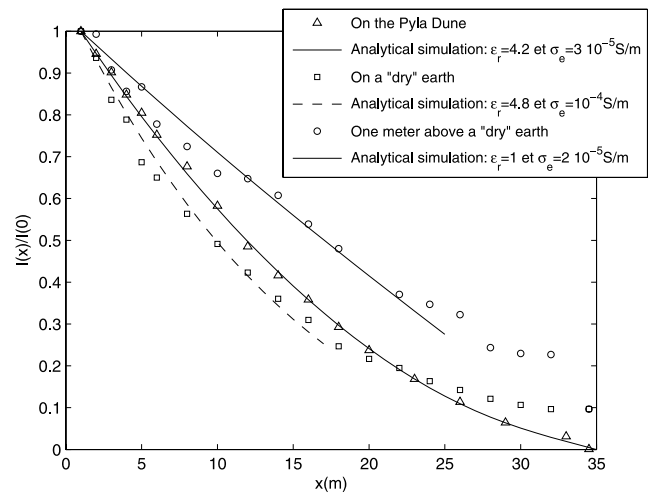


Figure 6. Comparison between measurements and an analytical model of the current distribution along the antenna. Measurements were performed in three locations: on the Pyla Dune, on a dry garden soil, and one meter above. Simulations curves correspond to the best fit to experimental data.

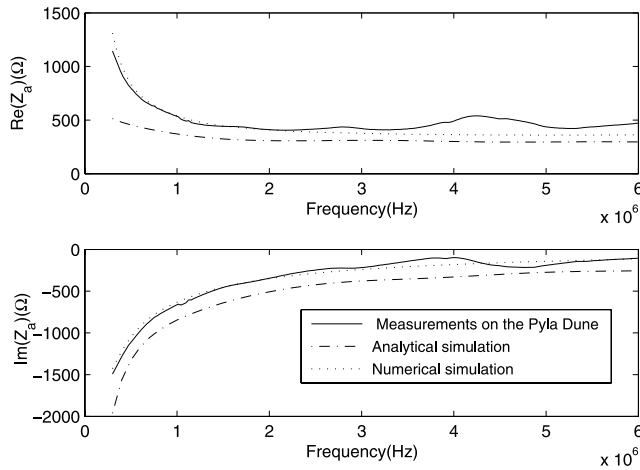


Figure 7. Comparison between the antenna impedance measured in the Pyla Dune and the analytically and numerically computed impedances. The numerically simulated curve corresponds to the best fit of experimental data.

puting the electrical parameters of the soil material can be easily done with such set of results used as abaci.

[70] As shown in section 3.3, the antenna impedance is virtually insensitive to the conductivity of the subsurface at high frequencies (above ~ 1.5 MHz) while it is significantly affected by the relative dielectric constant. Therefore ϵ_r is determined by a least squares fit of the measured real and imaginary parts of the self antenna impedance on the numerical model for frequencies larger than ~ 1.5 MHz. Using the inferred value of the relative permittivity, the conductivity of the soil is deduced from a fit of the measurements below ~ 1.5 MHz. Finally a best fit over the whole bandwidth with the previously determined ϵ_r and σ_e as starting values is performed.

[71] Such a method was used to analyze measurements made on the Antarctic ice shelf. Figure 9 displays the comparison between the measured, analytically and numerically computed real and imaginary parts of the antenna impedance. As aforementioned, in the frequency range of interest, the electromagnetic parameters of the ice are practically independent of frequency and we have thus assumed, in our modeling, a constant value of the electric permittivity and conductivity.

[72] The fitted parameters are $\epsilon_r = 3$ and $\sigma_e = 10^{-5}$ S/m, thus in very good agreement with the published values for ice under similar temperature conditions (see section 5.1.3).

[73] The error on the measurements can be reliably estimated as: $\frac{\Delta \text{Re}(Z_a)}{\text{Re}(Z_a)} = 2\%$ and $\frac{\Delta \text{Im}(Z_a)}{\text{Im}(Z_a)} = 6\%$. The numerical model yields quantitative information on the sensitivity of the antenna impedance to the variation of the geoelectrical parameters ϵ_r and σ_e . The resulting errors on the fitted parameters are: $|\Delta \epsilon_r| = 0.25$ and $|\Delta \sigma_e| = 3 \cdot 10^{-5}$ S/m.

[74] We can note that the relative error on the computed relative dielectric permittivity is very satisfying ($\sim 8\%$). In

contrast, the electric conductivity is obtained with less relative accuracy in particular for very low conductivity.

6. Summary and Conclusion

[75] In this paper, we have presented a method to measure the geoelectrical parameters of the upper layer of planetary subsurfaces that can be used with the HF GPR TAPIR. It is based on retrieving the relative permittivity and the conductivity of the investigated soil from the measured characteristics of antenna namely its impedance. This study led us to develop an analytical and a numerical model of the resistively loaded antennas that are used on the TAPIR ground-penetrating radar. The analytical approach allowed us to investigate the role of the electromagnetic parameters of the superficial soil on antenna characteristics. It reproduces quite properly the current profile along the antenna but, due to its simplicity, provides results on the antenna impedance that are inferior to those obtained with the numerical model. The numerical model, based on a FDTD code, is able to accurately simulate the antenna impedance and in particular its frequency profile. It provides a simple way to measure the permittivity and, with somehow less accuracy, the conductivity of the first meter of the soil. Values of ϵ_r and σ_e deduced from measurements over various soil conditions (ice and sand) are in very good agreement with published values or with actual measurements of the soil. Uncertainties on the inferred parameters have been evaluated. Our approach which can be implemented on a HF GPR, appears as a very promising method to retrieve the electrical properties of the soil with performances. More work is being done to improve the accuracy of the experimental measurements and to take into account the presence of magnetic materials in the soil. This can be of prime importance for an instrument on Mars. Since the Martian soil is expected to have a very low moisture content, we tested our parameter estimation procedure in

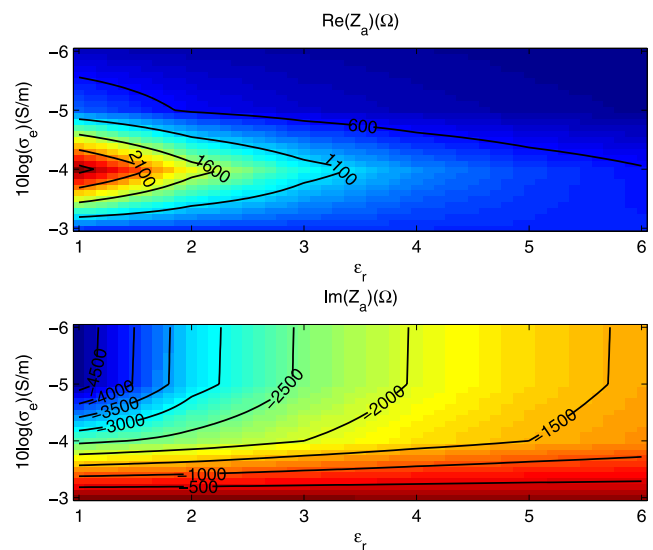


Figure 8. Numerically computed real and imaginary parts of the antenna self impedance as functions of the relative permittivity ϵ_r and of the conductivity σ_e of the shallow subsurface at the operating frequency of 1 MHz.

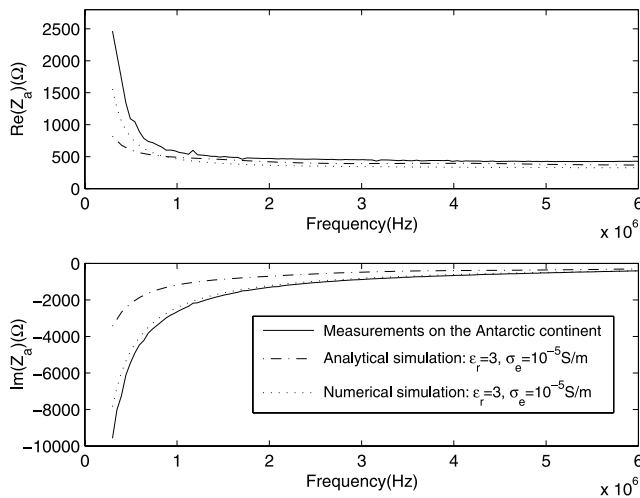


Figure 9. Comparison between the antenna impedance measured over the Antarctic ice shelf and the analytically and numerically computed impedances. The numerically simulated curve corresponds to the best fit of experimental data.

dry conditions. We plan to extend our work to a wider range of soils with possibly larger conductivities. Moreover, in this initial study, we assumed that the subsurface is homogeneous; it will be interesting to explore the effect of a fine scale layering, of a horizontal variability and of the presence of local heterogeneities under the antenna. Such investigation has been discarded to first order since we provided evidence that electromagnetic parameters derived from our procedure are only typical of the first meter of the soil thus a thin layer of the subsurface.

[76] **Acknowledgment.** The present work has been undertaken under the auspices of CNES grants 793/CNES/99/7947 and 737/CNES/00/8261.

References

- Baker, V. R. (2001), Water and the Martian landscape, *Nature*, 412(6843), 228–236.
- Barbin, Y. (1996), PRISM, le radar géophysique de l'aérostat martien, Ph.D., Serv. d'Aéron. du CNRS, Verrière-le-Buisson, France, Dec.
- Bauchet, G. (2004), Etude théorique et validation expérimentale de l'analyse électromagnétique d'un radar destiné au sondage du sous-sol martien, Ph.D., Univ. de Limoges, Limoges, France, Dec.
- Berenger, J. P. (1994), A perfectly matched layer for the absorption of electromagnetic waves, *J. Comput. Phys.*, 114, 185–200.
- Berenger, J. P., B. Martinat, and A. Reineix (2000), Reflection from PMLs in lossy media, URSI Session 105, vol. 3, p. 397, Int. Union of Radio Sci., Salt Lake City, 16–20 July.
- Berthelie, J. J., et al. (2000), The GPR on NETLANDER, *Planet. Space Sci.*, 48(12–14), 1161–1180.
- Berthelie, J. J., et al. (2003), GPR, a ground-penetrating radar for the Netlander mission, *J. Geophys. Res.*, 108(E4), 8027, doi:10.1029/2002JE001866.
- Berthelie, J. J., S. Bonaimé, V. Ciarletti, R. Clairquin, F. Dolon, A. Le Gall, D. Nevejans, R. Ney, and A. Reineix (2005), Initial results of the Netlander imaging ground-penetrating radar operated on the Antarctic Ice Shelf, *Geophys. Res. Lett.*, 32, L22305, doi:10.1029/2005GL024203.
- Besse, S. (2004), Etude théorique de radars géologique: Analyses de sols, d'antennes et interprétation des signaux, Ph.D., Univ. de Limoges, Limoges, France, Sept.
- Ciarletti, V., B. Martinat, A. Reineix, J. J. Berthelie, and R. Ney (2003a), Numerical simulation of the operation of the GPR experiment on NETLANDER, *J. Geophys. Res.*, 108(E4), 8028, doi:10.1029/2002JE001867.

- Ciarletti, V., J. J. Berthelie, R. Ney, S. Bonaimé, F. Dolon, A. Reineix, G. Bauché, and E. Heggy (2003b), Experimental validation of a ground penetrating radar dedicated to the Martian subsurface exploration — The Pyla sand dune, paper presented at IEEE International Geoscience and Remote Sensing Symposium, IGARSS2003, Inst. of Electr. and Electron. Eng., Toulouse, France, 21–24 July.
- Clifford, S. M. (1993), A model for hydrologic and climatic behavior of water on Mars, *J. Geophys. Res.*, 98, 10,973–11,016.
- De Jongh, R. V., A. G. Yarovoy, L. P. Ligthart, I. V. Kaploun, and A. D. Schukin (1998), Design and analysis of new GPR antenna concepts, paper presented at GPR'98, 7th International Conference on Ground Penetrating Radar, Univ. of Kans., Lawrence, 27–30 May.
- Fanale, F. P., J. R. Salvail, A. P. Zent, and S. E. Postawko (1986), Global distribution and migration of subsurface ice on Mars, *Icarus*, 67, 1–18.
- Fratticcioli, E., R. Sorrentino, A. Yarovoy, and L. Ligthart (2004), Permittivity evaluation for a vertically stratified soil using a GPR antenna, in *Proceedings of the Tenth International Conference on Ground Penetrating Radar*, edited by E. C. Slob, A. Yarovoy, and J. Rhebergen, pp. 727–730, Delft Univ. of Technol. Press, Delft, Netherlands.
- Fujita, S., T. Matsuoka, T. Ishida, K. Matsuoka, and S. Mae (2000), A summary of the complex dielectric permittivity of ice in the megahertz range and its applications for radar sounding of polar ice sheets, in *The Physics of Ice Core Record*, edited by T. Hondoh, Hokkaido Univ. Press, Sapporo, Japan.
- Hargraves, R. B., D. W. Collinson, R. E. Arvidson, and C. R. Spitzer (1977), The Viking magnetic properties experiments: Primary results, *J. Geophys. Res.*, 82, 4547–4558.
- Heggy, E., P. Paillou, G. Ruffie, J. M. Malezieux, F. Costard, and G. Grandjean (2001), On water detection in the Martian subsurface using sounding radar, *Icarus*, 154, 244–257.
- Helbert, J., and J. Benkoff (2005), Beyond the equilibrium paradigm—Glacial deposits in the equatorial region of Mars, *Lunar Planet. Sci.*, XXXVI, Abstract 1352.
- Holland, R., and L. Simpson (1981), Finite-difference analysis EMP coupling to thin struts and wires, *IEEE Trans. Electromagn. Compat.*, EMC-23(2), 88–97.
- Huisman, J. A., S. S. Hubbard, J. D. Redman, and A. P. Annan (2003a), Measuring soil water content with ground penetrating radar: A review, *Vadose Zone J.*, 2, 476–491.
- Huisman, J. A., J. J. C. Snepvangers, W. Bouten, and G. B. M. Heuvelink (2003b), Monitoring temporal development of spatial soil water content variation: Comparison of ground penetrating radar and time domain reflectometry, *Vadose Zone J.*, 2, 519–529.
- Kanda, M. (1978), A relatively short broadband antenna with tapered resistive loading for picosecond pulse measurements, *IEEE Trans. Antennas Propag.*, AP-26(3), 439–447.
- King, R. W. P., and G. S. Smith (1981), *Antenna in Matter: Fundamentals, Theory and Applications*, MIT Press, Cambridge, Mass.
- Lambot, S., E. C. Slob, I. van den Bosch, B. Stockbroeckx, and M. Vanclooster (2004), Modeling of ground-penetrating radar for accurate characterization of subsurface electric properties, *IEEE Trans. Geosci. Remote Sens.*, 42, 2555–2568.
- Lestari, A. A., A. G. Yarovoy, and L. P. Ligthart (2000), Adaptive antenna for ground penetrating radar, paper presented at GPR 2000, 8th International Conference on Ground Penetrating Radar, Gold Coast, Australia, 23–26 May.
- Leuschen, C., S. Clifford, and P. Gogineni (2003), Simulation of a surface-penetrating radar for Mars exploration, *J. Geophys. Res.*, 108(E4), 8035, doi:10.1029/2002JE001875.
- Ligthart, L. P., A. G. Yarovoy, A. A. Lestari, A. D. Schukin, and I. V. Kaploun (2002), GPR antenna development in IRCTR, paper presented at XXVIIth General Assembly of the International Union of Radio Science, Maastricht, Netherlands, 17–24 Aug.
- Luebbers, R. J., F. Hunsberger, K. S. Kunz, and M. Schneider (1990), A frequency dependent finite difference time domain formalism for dispersive media, *IEEE Trans. Electromagn. Compat.*, EMC-32, 222–227.
- Malin, M., and K. Edgett (2000), Evidence for recent groundwater seepage and surface runoff on Mars, *Science*, 288, 2330–2335.
- Martinat, B. (2001), Etude électromagnétique du GPR de NETLANDER destiné au sondage du sous-sol Martien, Ph.D. thesis, Univ. de Limoges, Limoges, France, Sept.
- Ney, R., S. Bonaimé, F. Dolon, D. Nevejans, R. Clairquin, C. Duvanaud, B. Martinat, J. J. Berthelie, and V. Ciarletti (2003), A ground penetrating radar for Mars exploration, the GPR Experiment on Netlander, paper presented at Ninth International Conference on HF Radio Systems and Techniques, Univ. of Bath, Bath, U.K., 23–26 June.
- Ori, G. C., and F. Oglioni (1996), Potentiality of the ground-penetrating radar for the analysis of the stratigraphy and sedimentology of Mars, *Planet. Space Sci.*, 44(11), 1303–1315.

- Reppert, P. M., F. D. Morgan, and M. N. Toksöz (2000), Dielectric constant determination using ground-penetrating radar reflection coefficients, *J. Appl. Geophys.*, *43*, 189–197.
- Roden, J. A., and S. Gedney (1997), Efficient implementation of the uniaxial based PML media in three-dimensional non-orthogonal coordinates using the FDTD technique, *Microwave Opt. Technol. Lett.*, *14*(2), 71–75.
- Shen, L. C., and R. W. P. King (1965), Correction to the cylindrical antenna with non reflecting resistive loading by Wu and King, *IEEE Trans. Antennas Propag.*, *AP-13*(6), 998.
- Squyres, S. W., S. M. Clifford, R. O. Kuzmin, J. R. Zimbelman, and F. M. Costard (1992), Ice in the Martian regolith, in *Mars*, edited by H. H. Kieffer et al., pp. 523–554, Univ. of Ariz. Press, Tucson.
- Van Overmeeren, R. A., S. V. Sariowan, and J. C. Gehrels (1997), Ground penetrating radar for determining volumetric soil water content: Results of comparative measurements at two test sites, *J. Hydrol.*, *197*, 316–338.
- Wait, J. R. (1972), Theory of wave propagation along a thin wire parallel to an interface, *Radio Sci.*, *7*(6), 675–679.
- Wright, D. L., and J. F. Prewitt (1975), Radiating dipole antenna with tapered impedance loading, *IEEE Trans. Antennas Propag.*, *23*(11), 811–814.
- Wu, T. T., and R. W. P. King (1965), The cylindrical antenna with nonreflecting resistive loading, *IEEE Trans. Antennas Propag.*, *13*, 369–373.
- Wu, T. T., and L.-C. Shen (1967), Cylindrical antenna with tapered resistive loading, *Radio Sci.*, *2*(2), 191.
- Yee, K. S. (1996), Numerical solution of initial boundary value problems involving Maxwell's equations in isotropic media, *IEEE Trans. Electromagn. Compat.*, *AP-14*(4), 302–307.

J. J. Berthelie, V. Ciarletti, C. Corbel, F. Dolon, A. Le Gall, and R. Ney, Centre d'Etudes des Environnements Terrestre et Planétaires (CETP/IPSL), 4, Avenue de Neptune, Saint-Maur, F-94107, France. (alg@cetp.ipsl.fr)
A. Reineix, XLIM/OSA/Projet CEM, Faculté des Sciences, 123, avenue Albert Thomas, F-87060, Limoges Cedex, France.